JOM, Vol. 71, No. 5, 2019
https://doi.org/10.1007/s11837-019-03423-w

TECHNICAL ARTICLE

Matte Entrainment by SO_2 Bubbles in Copper Smelting Slag

XIANGFENG CHENG,[1] ZHIXIANG CUI,[2] LEONEL CONTRERAS,[3] MAO CHEN,[1,4] ANH NGUYEN,[1] and BAOJUN ZHAO[1]

1.—School of Chemical Engineering, The University of Queensland, Brisbane 4072, Australia. 2.—Dongying Fangyuan Nonferrous Metals Co. Ltd, Dongying 257000, China. 3.—National Copper Corporation of Chile, 8320000 Santiago, Chile. 4.—e-mail: mao.chen@uq.edu.au

The attachment of copper matte by bubbles in slags, during the copper smelting process, plays a key role in the copper loss. This paper aims to provide an in-depth insight into the copper matte entrainment by bubbles in the copper production. The bubble size distribution and matte film thickness as well as the bubble detachment height were considered based on industrial and laboratory slag samples. The results indicated that most SO_2 micro-bubbles in both slag samples were below 650 μm, which could penetrate the interface and thus transport matte into the slag phase. The matte film thickness surrounding the micro-bubbles tended to be less than 30 μm and became thinner with increasing bubble size. Furthermore, micro-bubbles larger than 350 μm could theoretically rise by 0.5 m in the slag phase even with the drag force of the matte droplets.

INTRODUCTION

The smelting process as one of the important steps in the pyrometallurgical copper-making process to stratify copper matte from slag in the smelting furnace through oxidization of copper concentrates by oxygen-enriched air. The bottom-blown copper smelter and side-blown copper smelter (e.g., Noranda furnace and Teniente Converter, TC) using horizontal cylindrical vessels are some of the widely used copper smelting techniques. Both furnaces can be roughly sectioned into two zones, i.e., a reaction zone and a settlement zone. After fierce oxidization in the reaction zone, matte and slag will stratify in the settlement zone and then be discharged separately from the smelting furnace. However, the copper matte droplets present in the discharged slags cause losses of copper and lead to significant financial losses. The average copper content in the bottom-blowing smelting furnace (BBF) slag is reported to be around 3 wt.%,[1] whereas the copper content in TC slag can be up to 12 wt.%.[2,3]

A series of SEM images of industrial slag samples including BBF and TC slags were presented in our previous studies.[4] Theoretically, the Cu losses in smelting slags include the mechanically entrained discrete matte droplets and chemically dissolved Cu.[5–7] The analytical results of liquid slag composition by electron probe micro-analyzer show that approximately 0.5–0.6% Cu is distributed in the liquid slag, which is much smaller than the total losses in BBF (3%) and TC slags (12%). Thus, the mechanically entrained matte contributes greatly to the total matte loss in the slag phase. The preliminary analysis of industrial slag samples shows that copper matte entrainment in discharged smelting slags may originate from the following sources: (1) unreacted copper concentrate droplets; (2) precipitations of copper sulfide from the slag when solubility decreases as the bath temperature falls along the furnace; (3) attachment of matte droplets to spinel particles; and (4) mass transfer caused by gas bubbles.[2,4]

Due to the insufficient oxidization of a small proportion of copper mattes in the reaction zone, many SO_2 bubbles would be produced in the matte phase during the further oxidization process in the settlement zone. The analyses of industrial slag samples indicate that 15% and 11% matte droplets are attached to gas bubbles in BBF and TC slags, respectively, which could demonstrate that SO_2 bubbles rising across the matte–slag interface would cause copper matte entrainment in slag.[4] The SO_2 bubble generation mechanism in the matte phase in the settlement zone of the smelting furnace is expressed by:

(Published online March 13, 2019)

$$CuFeS_{2(s)} + O_{2(g)} + SiO_{2(s)} \rightarrow (Cu-Fe-S)_{(l)} + FeO-SiO_{2(l)} + SO_{2(g)} + heat \quad (1)$$

The studies on the bubble transport effect on lower liquid entrainment through the liquid–liquid interface tend to start from a single bubble, and the single bubble rising behaviors have been applied in numerous industrial applications, e.g., metallurgical processes,[8–11] nuclear reactor safety,[12] chemical process,[13,14] etc. The bubble transport behaviors through the liquid–liquid interface have been widely studied by cold model experiments and numerical simulations.[6,15–18] Mercier et al.[15] studied the upper liquid viscosity effects on lower liquid layer detachment height from bubbles and the ratio of volume to bubble volume. Greene and Yasuhiko explored the critical bubble sizes to pass through the interface of two immiscible liquids and entrain the lower liquid into the upper phase.[9,16,19] Kemiha et al.[18] compared the bubble size effects on the time spent at the liquid–liquid interface. Travis et al.[20] systematically categorized the bubble flow regimes into four groups and developed nondimensional numbers to characterize the flow regimes which vary significantly with bubble size during the bubble passage through a liquid–liquid interface.

Based on previous research, large gas bubbles usually larger than 3 mm in diameter tend to entrain lower liquid in the form of perceptible discrete droplets by a large momentum at the interface in cold model experiments. However, small gas bubbles tend to cross the interface cleanly without perceptible liquid droplets attached when interface ruptures gradually. Thus, the study on the lower liquid entrainment by small gas bubbles is ignored due to the incorrect assumption that the micro-bubbles are unable to pass and transport lower liquid through the interface.[9]

However, the pressure from the bubble and the mobile interface would cause the film to drain gradually inbetween and the bubbles could eventually penetrate the interface due to the decreasing interfacial tension with the thinning film.[20,21] The rising small gas bubbles crossing the interface carry a thin film of dense liquid on their surface instead of perceptible discrete droplets by large bubbles. Thus, the dense liquid entrainment process by small bubbles could not be simulated by large bubbles in conventional cold model experiments. The film spreading coefficient and flotation coefficient involving liquid surface tensions and interfacial tension could predict the film stability on the bubble surface.[8]

The main objective of the present study is to fill the perception gap on thin lower liquid film entrainment by micro-bubbles at the micron scale, which cannot be observed by traditional high-speed imaging in cold model experiments. The relationship between matte film thickness and attached bubble size and the expected detachment height are evaluated in this paper by high-temperature experiments.

EXPERIMENTAL

The industrial slag and matte samples were provided by Shandong Fangyuan Nonferrous Metals, China, and their chemical compositions are shown in Table I. It can be seen that the slag sample contains 26.5 wt.% SiO_2 and 3.2 wt.% Cu_2O and that the matte sample contains 72.7 wt.% Cu. Moreover, the chemicals Cu_2O (≥ 99.99%) and FeS (≥ 99.9%; both Sigma-Aldrich, USA) were also used in the present study to generate SO_2 bubbles according to Eq. 2. A three-layer sample was prepared (see Fig. 1): 5 g of slag layer at the top, 1 g of a matte layer in the middle and a mixture of 0.5 g Cu_2O (≥ 99.99%) and 0.5 g FeS (≥ 99.9%) at the bottom in an alumina crucibles (inner diameter: 16 mm, height: 40 mm). The pelletized Cu_2O and FeS mixture was placed at the bottom of the crucible to generate SO_2 bubbles to simulate the bubble transportation process in the smelting furnace.

$$Cu_2O + FeS \rightarrow Cu-Fe-S\ (matte) + SO_2 \uparrow \quad (2)$$

The experiments were conducted in a vertical tube furnace in Ar atmosphere (99.999%; Coregas, Australia), as shown in Fig. 1a. The specimen was first placed in the furnace at 600°C to dry for 30 min, and then heated at 5°C/min to 900°C. The three-layer sample was treated at a heating rate of 10°C/min and then kept at 1200°C for 10 min to release as many bubbles as possible. The crucible was then lowered slowly to the cold end of the furnace and fast-quenched by high-purity Ar gas. Approximately 900 bubbles observed from the SEM images were used to evaluate matte entrainment by the gas bubbles, and a typical SEM image of the sample is shown in Fig. 2. The image analysis software (ImageJ) was used to measure the bubble and matte size distribution.

RESULTS AND DISCUSSION

Attachment Between Matte Droplets and Gas Bubbles

The typical microstructure of the laboratory sample is shown in Fig. 2. It should be noted that the sizes of the SO_2 bubbles at the micron scale in the laboratory samples are of the same order of magnitude as those in the industrial slag samples (BBF and TC slags).

The results show that numerous SO_2 bubbles are scattered and suspended in the slag, among which 91% volume proportion of matte droplets are associated with the gas bubbles. The laboratory experiment demonstrates that SO_2 micro-bubbles have the ability to transport copper matte into the slag layer. The attachment between the matte droplets and the gas bubbles could remain stable in the slag

Table I. Chemical composition of industrial slag and matte samples (wt.%)

Slag	"FeO"	SiO_2	Cu_2O	CaO	Al_2O_3	MgO	S	As_2O_3	PbO	ZnO	MoO_3
	60.6	26.5	3.2	1.3	3.3	1.2	0.7	0.1	0.6	2.4	0.1
Matte	Fe	Cu	S	Zn	As	Pb					
	5.0	72.7	21.9	0.1	0.0	0.2					

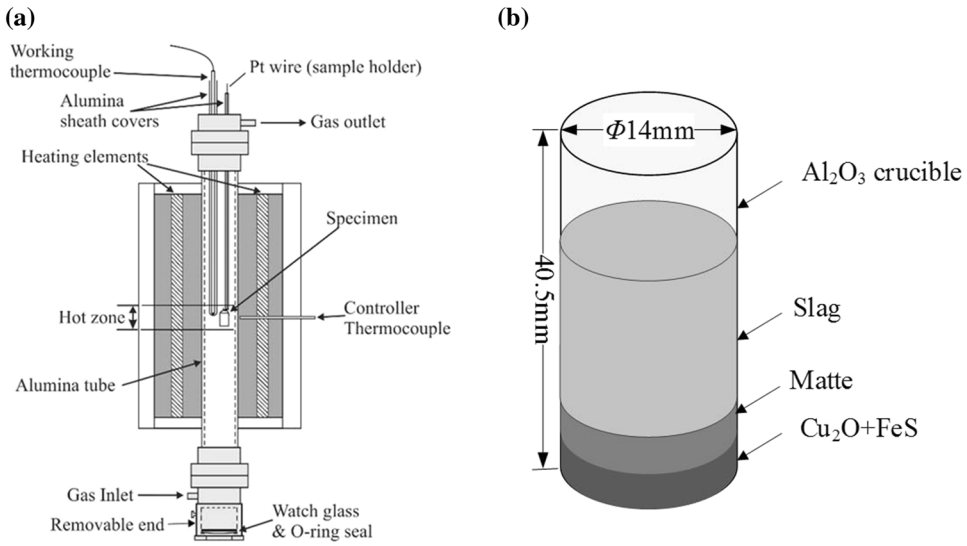

Fig. 1. (a) Schematic of the tube furnace, (b) the sample structure in the crucible.

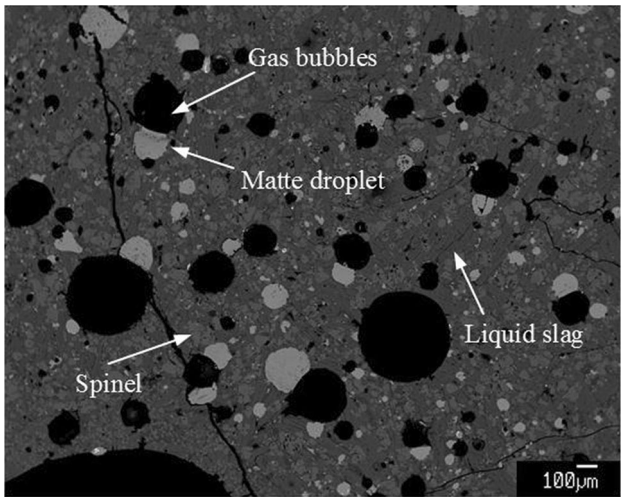

Fig. 2. Typical microstructure of slag in the high-temperature experiment.

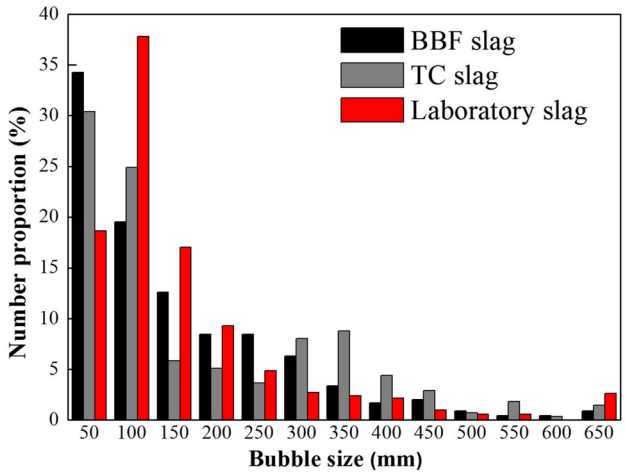

Fig. 3. The bubble size distribution in industrial and laboratory slag samples.

phase at 1200°C. However, the volume proportions of the matte attachments to the gas bubbles in industrial slags (BBF slags 15% and TC slags 11%)[4] are much lower than that in the laboratory slags. Therefore, the matte droplets probably eventually detach from the SO_2 bubbles in the slag phase and then settle down, while the bubbles will keep rising, and finally rupture.

Bubble Size Distribution in Slag Samples

As bubble size plays a significant role in determining the matte entrainment regimes,[20] it is necessary to have a general understanding of bubble size distribution in the slag. The bubbles and copper matte droplets are regarded as spherical in shape, as shown in Fig. 2, in order to measure their size in SEM photographs. Figure 3 shows the

comparisons of bubble diameters and the number in both industrial and laboratory slags.

Figure 3 shows that majority of gas bubbles are smaller than 650 μm in the slag samples, which is far less than the normal bubble size studied in previous cold model simulation experiments to simulate bubble penetration behaviors through an immiscible liquid interface.[11,16,18,19] Assuming the densities of the BBF slags and mattes in this experiment are $\rho_{slag} = 3.5 \times 10^3$ kg/m^3 and $\rho_{matte} = 4.7 \times 10^3$ kg/m^3, respectively, and the interfacial tension $\sigma_{12} = 0.1$ N/m, the critical bubble entrainment diameter to cross the slag–matte interface and transport the matte into the slag would be 4.6 mm, according to Greene's theory.[9] Nevertheless, the micro-bubbles presentation in the slag phase contradicts this theory, and demonstrates that micro-bubbles at micron scale could also pass through the interface and entrain matte into the slag.

Micro-bubbles actually tend to first dwell at the interface between immiscible liquids and then pass through without perceptible lower liquid attached, based on observation results from the present cold model experiments and Travis's analysis on bubble flow regimes.[20] During the dwelling period, some micro-bubbles will probably experience coalescence to form large bubbles at the interface, and these large gas bubbles then rise rapidly through the whole slag phase. Therefore, the possibility of large bubble existing in the slags could not be eliminated. Here, the present research focuses mainly on the bubbles at micron scale observed in the slags.

The Matte Film Thickness on the Bubble Surface

To quantify the matte entrainment volume by micro-bubble transport behaviors, the relationship between matte film thickness and bubble size was investigated. The dense liquid film is believed to be surrounding the gas bubble surface after penetrating the interface before subsequent behaviors in the lighter liquid, e.g., matte attachment transforms on the gas bubbles, depending on the properties of the two superposed liquids.[8] Assuming that the matte droplets are originally evenly spread on the micro-bubble surface after passing through the interface, the matte film thickness refers to the thickness of the attached matte layer enveloping the bubble surface. To further verify the bubble transport capability to lift attached matte droplets effectively in each attachment, the preliminary evaluation on effective matte entrainment by gas bubbles was carried out based on the statistics of the laboratory experimental data through force balance analysis, as shown in Fig. 4.

Figure 4 shows the rising bubble force balance with the drag force from the attached matte droplets. The prerequisite for a gas bubble to float matte droplets should be that the bubble buoyancy force, F_B, should be larger than the matte droplets drag force, i.e., $F_B > G_{matte} - F_M$. The effective film thickness refers to the matte film thickness on the surface of the bubbles with sufficient buoyancy force to lift matte droplets, and the ineffective film thickness is the matte film thickness on the surface of the bubbles failing to carry matte droplets upwards. The analysis of force balance acting on gas bubbles is as follows:

$$\rho_{slag} g V_g > (\rho_{matte} - \rho_{slag}) g V_{matte} \tag{3}$$

$$\frac{d_g}{d_{matte}} = \sqrt[3]{\frac{V_g}{V_{matte}}} > \sqrt[3]{\frac{\rho_{matte} - \rho_{slag}}{\rho_{slag}}} \tag{4}$$

where V_g and V_{matte} are the bubble and matte volumes, d_g and d_{matte} are the gas bubble and matte droplet diameters, and ρ_{matte} and ρ_{slag} are matte and slag densities, respectively.

The result shows that more than 89% attachments between mattes and bubbles are effective, which means that the majority of the bubbles observed could lift the matte droplets by buoyancy force. Then, the matte film thickness could be calculated based on the matte droplet volume and the attached gas bubble size, as shown in Fig. 5.

Figure 5a shows that the theoretical matte film thicknesses on all the gas bubbles are smaller than 100 μm. However, some gas bubbles are probably from the ruptured large bubbles and subsequently attached to the matte droplets in the slag phase. Thus, the gas bubble buoyancy force fails to lift the attached matte droplets based on the force balance analysis, as shown in Fig. 4. Through removing a few ineffective attachments between the bubbles and the matte droplets, the effective matte film thicknesses are smaller than 30 μm. Generally, the thin dense liquid film could be neglectable for bubbles at the millimetre scale but vital for numerous bubbles of micron size.

For the relatively larger bubbles, the matte film tends to be thinner, while the film thickness varies for bubbles of small size, as shown in Fig. 5a. This is mainly because the matte surface tension could not support the thicker matte film surrounding the larger gas bubbles due to the large surface area, while this situation does not necessarily occur for small gas bubbles. However, the maximum matte entrainment volume increases with increasing bubble size, as shown as Fig. 5b, which indicates that larger bubbles could transport more matte droplets into the slag phase even enveloped with a possible thinner matte film thickness.

The Detachment Height Prediction of Bubbles Attached to Gas Bubbles

The matte detachment height, H, from the rising gas bubbles is defined as the maximum rising height of matte droplets when detaching from the attached gas bubbles in the slag phase. H is obviously an

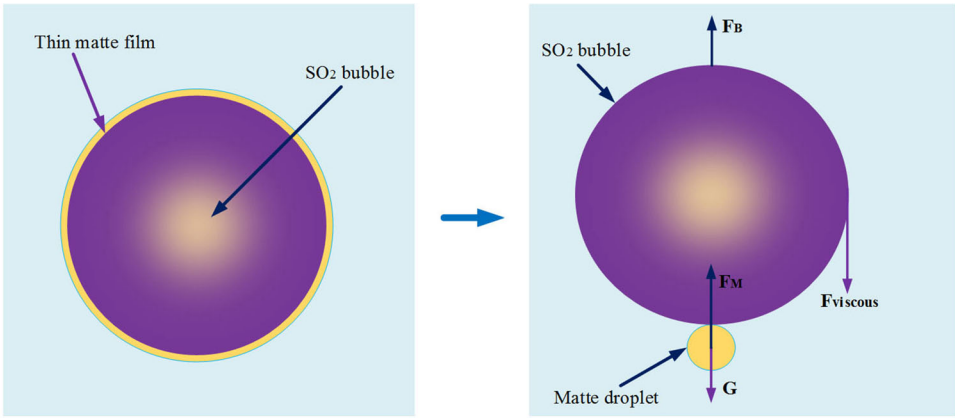

Fig. 4. The force balance of gas bubbles attached to matte droplets in the slags (FB—Bubble buoyancy force; G—Matte gravity; FM—Matte buoyancy force).

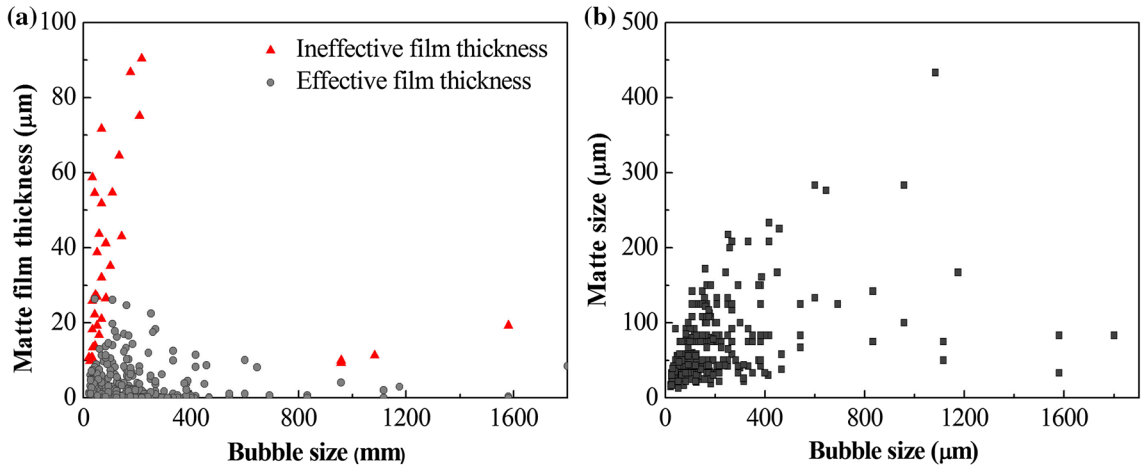

Fig. 5. (a) The matte film thickness prediction on bubbles, (b) the matte size in diameter attached to bubbles.

important parameter of great concern to many researchers as it determines the matte entrainment possibility in the slag phase. Despite many difficulties in directly measuring the H of the thin matte film from gas bubbles, it could still be predicted by the stable attachment time between the matte and the bubbles according to the Stoke's equation. From the preliminary investigation of the attachment between the matte droplets and the gas bubbles, the attachment remains stable for at least 10 min in the slag phase with a height of 20 mm. If time and slag thickness allow, the matte droplets with bubbles would rise continuously until being discharged with the slag from the smelting furnace. The minimum matte detachment height could be predicted by the attached bubble terminal velocity within 10 min in the slag phase.

From the above-mentioned SEM photographs, we can see that the spherical gas bubbles are rising in the slag with the drag force from the matte droplets. Assuming that the drag force from the matte droplets attached to the bubbles only includes the buoyancy force and gravity, and that the viscous force in slags can be neglected, a new Stoke's equation could be deduced by the bubble buoyancy force, bubble viscous force and matte droplet drag force, in accordance with Eq. 5. As the bubble size, d_g, and the corresponding attached matte droplets size, d_{matte}, are related, we can find the relationship between the bubble buoyancy force and the matte drag force based on the experimental data. The results show that the matte drag force, i.e., the difference between the matte buoyancy force and gravity accounts for less than 20% of the bubble buoyancy force in the 82% attachment between the bubbles and the matte droplets. Therefore, we can use the bubble buoyancy force to substitute the matte drag force to simplify the calculation of Eq. 5. Thus, the maximum bubble terminal rising velocity can be deduced by replacing the matte drag force with 20% bubble buoyancy force, as in Eq. 6.

$$3\pi\mu_{slag}d_g v = (\rho_{slag} - \rho_g)g\frac{\pi}{6}d_g^3 - (\rho_{matte} - \rho_{slag})g\frac{\pi}{6}d_{matte}^3 \quad (5)$$

then,

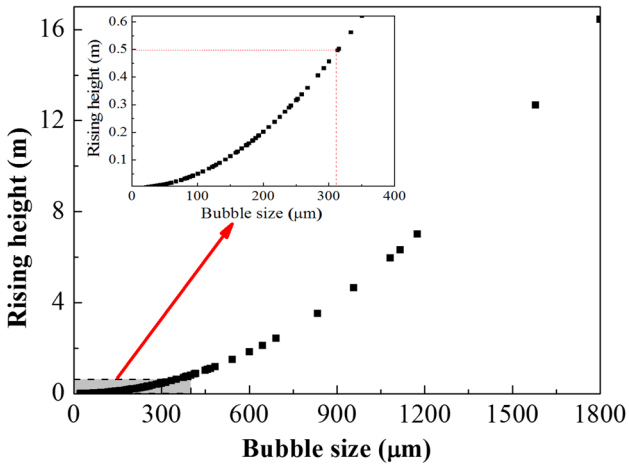

Fig. 6. The prediction of matte detachment height from rising gas bubbles in 10 min.

$$v = \frac{2}{45}\frac{(\rho_{slag} - \rho_g)}{\mu} g d_g^2 \quad (6)$$

where μ_{slag} is the slag dynamic viscosity, and v is the bubble terminal rise velocity in the slag phase. Thus, the preliminary prediction of bubble rising height can be shown as in Fig. 6.

From Fig. 6, it can be seen that the rising height of bubbles larger than 140 um accounting for 73% of total bubbles could reach up to 0.1 m in 10 min, and those larger than 200 um (17%) could rise above 0.2 m. The bubbles larger than 350 um (7%) could transport matte droplets through the whole 0.5-m slag phase in 10 min during the stable attachment period. Therefore, larger micro-bubbles tend to transport the matte higher and will increase the matte entrainment possibility in the slag. Considering the in-depth analysis of extremely slow matte droplet settlement in our previous study,[4] it can be concluded that micro-bubbles can still play a significant role in matte entrainment.

CONCLUSION

The micro-bubble influences on the copper matte entrainment in the slag phase have been discussed and the following conclusions were drawn:

(1) The copper matte mechanical entrainment by gas bubbles in the slag phase has been confirmed. Bubbles produced by further matte oxidization in the settlement zone are generally at the micron scale and can penetrate the matte–slag interface and transport matte into the slag phase.

(2) Total matte film thicknesses on the bubble surface are below 100 μm, and those the effective attachment are usually smaller than 30 μm. The matte film thickness is generally thinner on the larger bubbles and varies on the smaller bubbles. However, the larger gas bubbles tend to transport more matte into the slag in terms of matte entrainment volume.

(3) The majority of SO_2 micro-bubbles can transport matte droplets to a higher level in the slag, leading to matte entrainment in the slag phase considering the extremely slow matte settlement in the slag phase.

In the bath copper smelting process, if the oxidation does not complete in the reaction zone, further reaction in the matte will generate SO_2 gas in the settling zone of the smelting furnace. The matte droplets brought by the gas bubbles would not have enough time to settle and will be tapped with the slag, causing losses of copper. This important finding will enable the operators to understand the mechanisms of the matte droplets entering the slag. Proper actions to reduce or stop the entrainment of the matte droplets can be taken to control the copper loss in the smelting slag and increase the efficiency of the smelting process for primary copper production.

ACKNOWLEDGEMENTS

The authors would like to thank National Copper Corporation of Chile (Codelco), Dongying Fangyuan Nonferrous Metals (Fangyuan) and Australia Research Council for financial support through the ARC Linkage program. The authors also would like to thank China Scholarship Council (CSC) and The University of Queensland to provide Xiangfeng Cheng scholarship.

REFERENCES

1. B. Zhao, Z. Cui, and Z. Wang, *4th International Symposium on High-Temperature Metallurgical Processing* (2013), p. 3.
2. D. Poggi, R. Minto, and W.G. Davenport, *JOM* 21, 40 (1969).
3. M. Chen, L. Contreras, and B. Zhao, *Copper* 2016, 976 (2016).
4. X. Cheng, Z. Cui, L. Contreras, M. Chen, N. Anh, and B. Zhao (eds.), *8th International Symposium on High-Temperature Metallurgical Processing* (2017). https://doi.org/10.1007/978-3-319-51340-9_37.
5. N. Cardona, L. Hermandez, E. Araneda, and R. Parra, Evaluation of copper losses in the slag cleaning circuits from two Chilean smelters, in *Proceedings of Conference on Copper*, June 2010, pp. 2637–2654.
6. I.K. Suh, Y. Waseda, and A. Yazawa, *High Temp. Mater. Process. (Lond.)* 8, 65 (1988).
7. M. Schlesinger, M. King, K. Sole, and W. Davenport, *Extractive Metallurgy of Copper* (Oxford: Elsevier, 2011), p. 191.
8. R. Minto and W.G. Davenport, *Can. Min. Metall. Bull.* 65, 36 (1972).
9. G.A. Greene, J.C. Chen, and M.T. Conlin, *Int. J. Heat Mass Transf.* 31, 1309 (1988).
10. S.W. Ip and J.M. Toguri, *Metall. Mater. Trans. B* 23, 303 (1992).
11. M. Tanno, J. Liu, X. Gao, S.J. Kim, S. Ueda, and S. Kitamura, *Metall. Mater. Trans. B* 48, 2913 (2017).
12. R. Bonhomme, J. Magnaudet, F. Duval, and B. Piar, *J. Fluid Mech.* 707, 405 (2012).
13. K.K. Singh and H.-J. Bart, *Ind. Eng. Chem. Res.* 54, 9478 (2015).
14. N. Dietrich, S. Poncin, S. Pheulpin, and H. Li, *AIChE J.* 54, 594 (2008).
15. J.L. Mercier, F.M. Cunha, J.C. Teixeira, and M.P. Scofield, *J. Appl. Mech.* 41, 29 (1974).
16. G.A. Greene, J.C. Chen, and M.T. Conlin, *Int. J. Heat Mass Transf.* 34, 149 (1991).

17. G. Reiter and K. Schwerdtfeger, *ISIJ Int.* 32, 50 (1992).
18. M. Kemiha, E. Olmos, W. Fei, S. Poncin, and H.Z. Li, *Ind. Eng. Chem. Res.* 46, 6099 (2007).
19. Y.H. Mori, K. Komotori, K. Higeta, and J. Inada, *Can. J. Chem. Eng.* 55, 9 (1977).
20. T.S. Emery, P.A. Raghupathi, and S.G. Kandlikar, *Langmuir* 34, 6766 (2018).
21. A.V. Nguyen, H.J. Schulze, H. Stechemesser, and G. Zobel, *Int. J. Miner. Process.* 50, 97 (1997).